IOP Publishing Measurement Science and Technology
Meas. Sci. Technol. **36** (2025) 026307 (13pp) https://doi.org/10.1088/1361-6501/ada179

# Differential code biases estimation from Sentinel-6A GPS and Galileo combined observations

**Hui Peng**[1], **Shuanggen Jin**[1,2,3,*] **and Zilong Chen**[1]

[1] School of Remote Sensing and Geomatics Engineering, Nanjing University of Information Science and Technology, Nanjing 210044, People's Republic of China
[2] School of Surveying and Land Information Engineering, Henan Polytechnic University, Jiaozuo 454003, People's Republic of China
[3] Shanghai Astronomical Observatory, Chinese Academy of Sciences, Shanghai 200030, People's Republic of China

E-mail: sgjin@shao.ac.cn

Received 3 September 2024, revised 3 December 2024
Accepted for publication 19 December 2024
Published 10 January 2025

**Abstract**

Differential code bias (DCB) is the hardware delay in the ranging code of the global navigation satellite system (GNSS), which critically impacts ionospheric total electron content estimation, precise positioning and accurate timing. The GNSS receiver aboard the Sentinel-6A low Earth orbit satellite is a crucial payload for precise orbit determination and topside ionospheric studies, while the GNSS receiver DCB is one of the errors. In this paper, the DCB variations of both GNSS satellites and receivers are estimated and analyzed using dual-frequency observations from the Sentinel-6A GNSS receiver (GPS and Galileo) during different solar activity periods. The results show that DCB estimates from GPS and Galileo combined observations are significantly more accurate than those from single-system estimates. The combined estimate results show that the overall monthly mean differences between the DCB estimates of GPS and Galileo satellites and the reference values from the German Aerospace Center and the Chinese Academy of Sciences are stable at 0.31, 0.34, 0.15 and 0.19 ns, respectively. During the high solar activity, the mean difference between the combined estimation result and the reference value is 0.34 ns and 0.16 ns. The difference for the GNSS receiver DCB estimates between single-system and GPS + Galileo combined estimations is minimal, with mean differences within 0.11 ns. Using GPS + Galileo combined observations enhances the stability of the GNSS receiver DCB estimates by 7% and 32%, respectively when compared to single-system estimates. The GPS + Galileo combined observations provide a good DCB estimation for Sentinel-6A precise orbit determination and topside ionosphere modeling.

Keywords: DCB, GPS, Galileo, GNSS, Sentinel-6A

* Author to whom any correspondence should be addressed.

## 1. Introduction

In recent years, low Earth orbit (LEO) satellites equipped with dual-frequency global navigation satellite system (GNSS) receivers have become essential for orbit determination, topside ionospheric study and remote sensing (Jin *et al* 2024). These satellites can effectively measure topside ionospheric electron density in both space and time (Li and Jin 2023). The ionospheric delay is the significant GNSS error source, which can lead to large errors in both navigation and positioning (Jin *et al* 2004, 2006, Jin and Park 2007, Jin and Li 2018). When the total electron content (TEC) is extracted from dual-frequency GNSS observation data, the signal transmission delay caused by the hardware in the satellite and receiver is referred to as hardware delay (Jin *et al* 2022b). The difference between these delays at two signal frequencies, known as differential code bias (DCB), is a major error source in TEC estimation and can result in deviations of up to 8–30 TECU in precise navigation and timing (Jin *et al* 2012). Therefore, accurate estimation of DCBs for GNSS satellites and LEO satellite GNSS receivers is crucial to obtain unbiased topside ionospheric TEC (Zhong 2017). Various analysis centers, including the International GNSS Service (IGS), the German Aerospace Center (DLR), and the Chinese Academy of Sciences (CAS), have estimated TEC and GNSS satellite DCB using ground-based observational data (Wang 2023), while DCB products for LEO satellite GNSS receivers are currently unavailable. Due to the high velocity of LEO satellites in orbit and their rapid changes in latitude and local time, DCB estimation methods designed for ground-based GNSS receivers are not directly applicable to LEO satellite data processing. Therefore, estimating and analyzing DCB variations of GNSS receivers on LEO satellites is important and urgent for precise orbit determination, topside ionospheric modeling and space environment monitoring (Shi *et al* 2023, Wang *et al* 2023).

In current studies, the common method for estimating the DCB of LEO satellite GNSS receivers uses dual-frequency GNSS observational data with geometry-free (GF) combinations of pseudorange and carrier phase measurements (Sanz *et al* 2017). Zhong (2017) proposed that the TEC observed by LEO satellites tends to be minimal during nighttime or at high latitudes and extracted the lower quartile of the smallest observed TEC over all daily orbital periods and further adjusted this as the DCB result. While this approach is straightforward and computationally efficient, cycle slips and multipath effects significantly impact the LEO satellite observation data. Most researchers adopt a spherical symmetry assumption model by converting ionospheric TEC into vertical TEC (VTEC) using the corresponding mapping function (MF), thus reducing the number of unknown parameters. Subsequently, the official GNSS satellite DCB products released by the IGS analysis center were treated as true values and only the receiver DCB and VTEC parameters were estimated (Zhang and Tang 2014, Zhou *et al* 2022, Lin *et al* 2023). It is evident that this processing approach depends heavily on the accuracy of GNSS satellite DCB provided by the IGS analysis center. Consequently, the most commonly used method is to simultaneously compute the three unknown parameters using least squares, which has been extensively applied to estimate DCB for LEO satellites, including FY-3C (Li *et al* 2017), FY-3D (Li *et al* 2019), COSMIC-2 (Pedatella *et al* 2021), SWARM (Lin *et al* 2023), and GRACE-FO (Zhou *et al* 2022). Li *et al* (2019) first used BDS + GPS observation data from the FY-3D and FY-3C LEO satellites to jointly estimate the DCB of GNSS satellites and receivers, showing significant improvements in the accuracy and stability of DCB estimation for GPS and BDS satellites. The effect of DCB estimation on VTEC estimation, as well as the relationship between DCB variation, geomagnetic activity, and solar activity, are also investigated. Yuan *et al* (2021) employed multi-layer MFs by combining various LEO satellites at different altitudes to estimate the GPS receiver DCB and the ionospheric TEC, aiming to reduce mapping errors. Additionally, some researchers have performed joint data estimation for LEO satellite constellations at the same orbital altitude, such as the SWARM constellation (Lin *et al* 2023), GRACE-FO (Zhou *et al* 2022), Jason-2/3 (Li *et al* 2020), and Metop-ABC (Li *et al* 2021, Li and Jin 2023). However, most LEO satellites currently carry GPS receivers with only limited GNSS observation data.

The Sentinel-6A satellite, developed collaboratively by the European Space Agency and National Aeronautics and Space Administration (NASA), is a global ocean monitoring satellite that measures sea level height using an altimeter and supporting the study of climate change and ocean dynamics (Montenbruck *et al* 2021). The GNSS receiver on the satellite is utilized for precise orbit determination, but its DCB is not available. Accurate estimation of the GNSS receiver DCB can enhance precise orbit determination and topside ionospheric modeling as well as scientific applications (Jin *et al* 2022a).

In this paper, the DCBs of GNSS satellites and the GNSS receiver onboard the Sentinel-6A satellite are estimated and evaluated using GPS, Galileo and their combined observations based on the spherical harmonics method. The remainder of this paper is organized as follows. Section 2 introduces the data and the method. Section 3 estimates and evaluates the DCB of GNSS satellites and Sentinel-6A GNSS receiver from different systems and combined observations. Finally, the conclusions are given in section 4.

## 2. Data and methods

### 2.1. LEO data

The Sentinel-6A satellite orbits in a sun-synchronous path at an altitude of approximately 1336 km, providing ideal conditions for precise sea level measurements. This mission, a collaboration between the European Copernicus Program, NASA, and NOAA, monitors global sea level changes, ocean surface winds, and wave heights. Sentinel-6A is equipped with the advanced GEMINI GNSS receiver, supporting both GPS

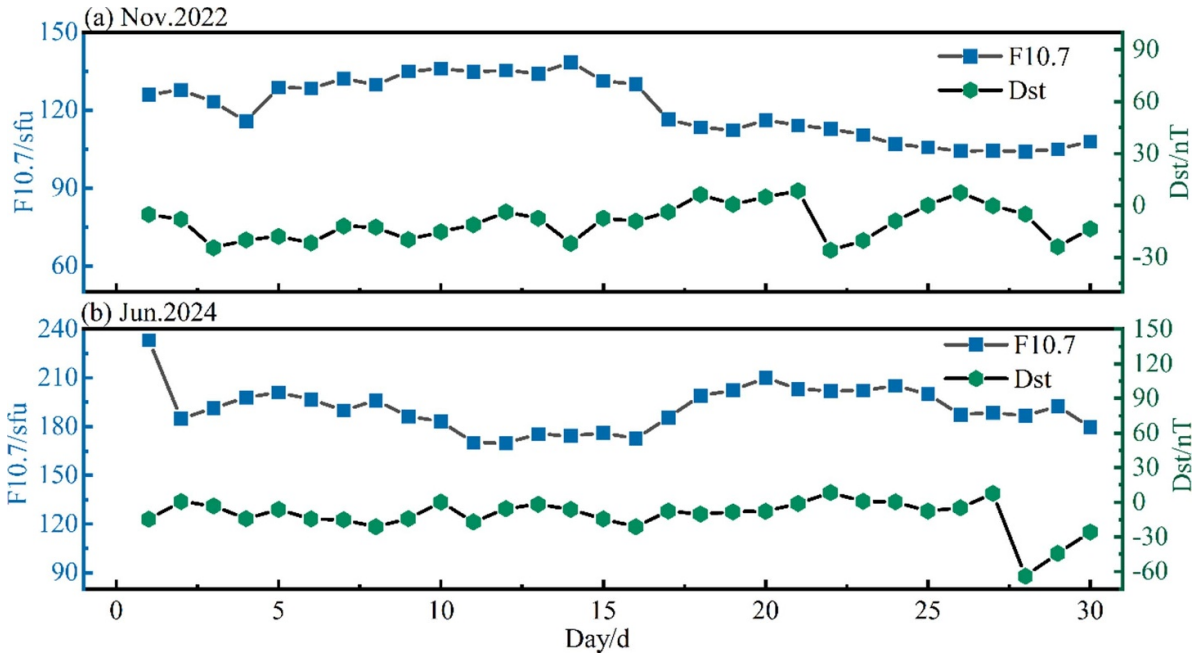


**Figure 1.** Distribution of F10.7 and Dst in June 2022 (a) and November 2024 (b).

and Galileo systems, which is capable of processing multi-frequency signals (L1, L2, L5, E1, E5, etc), enhancing positioning accuracy and anti-jamming capabilities. Using single-receiver ambiguity resolution techniques, it determines precise orbits in various configurations, such as GPS-only, Galileo-only, or combined GPS/Galileo.

This study used GNSS (GPS and Galileo) observations in November 2022 and June 2024 for DCB estimates. Considering the sensitivity of GNSS data from LEO satellites to space weather, observation periods with stable solar and geomagnetic activity, as well as those with high solar activity, were chosen to show the performance of the experiment. Additionally, LEO satellite observations and GNSS satellite orbital data were obtained from official websites.

The GNSS data from Sentinel-6A for November 2022 and June 2024 were analyzed. Figure 1 shows solar activity and geomagnetic indices for these periods. In November 2022, the F10.7 index ranged from 100 to 130 sfu, and the disturbance storm time (Dst) index remained above −30 nT. According to national standards, geomagnetic conditions were stable, and solar activity was moderate. In June 2024, the F10.7 index exceeded 150 sfu, indicating high solar activity.

### *2.2. GF combination and carrier phase-smoothed pseudorange*

This study combines pseudorange and carrier phase observations from the dual-frequency GNSS receiver on the Sentinel-6A LEO satellite to simultaneously estimate VTEC, GNSS satellite DCB, and GNSS receiver DCB as unknown parameters. The dual-frequency pseudorange and carrier phase observation equations for GNSS on LEO satellites are as follows (Jin *et al* 2012):

$$\begin{aligned} P^s_{r,i} &= \rho^s_r + c\left(\mathrm{d}t_r - \mathrm{d}t^s\right) + \left(40.28/f_i^2\right) I^s_r + c\left(\mathrm{d}_{r,i} + \mathrm{d}^s_i\right) + \Delta^s_r \\ L^s_{r,i} &= \rho^s_r + c\left(\mathrm{d}t_r - \mathrm{d}t^s\right) - \left(40.28/f_i^2\right) I^s_r + B^s_{r,i} + \Delta^s_r \end{aligned} \quad (1)$$

where $P^s_{r,i}$ and $L^s_{r,i}$ are the pseudorange and carrier phase observations at frequency $i$, respectively; The superscript $s$ and the subscript $r$ represents the serial numbers of GNSS satellites and LEO spaceborne GNSS receivers; $\rho^s_r$ is the geometric distance from the GNSS satellite to the receiver; $c$ is the speed of light, $\mathrm{d}t_r$ and $\mathrm{d}t^s$ are the clock offsets of the receiver and the satellite, respectively; $\alpha_i$ is the ionospheric delay conversion coefficient, given by $\alpha_i = \left(40.28/f_i^2\right)$, where $f$ is the frequency; $I^s_r$ is the slant TEC (STEC) along the line-of-sight from the GNSS satellite to the receiver; $\mathrm{d}_{r,i}$ and $\mathrm{d}^s_i$ are the hardware delays of pseudorange observations at frequency $i$ for the receiver and the satellite, respectively; $B^s_{r,i}$ is the ambiguity bias in the carrier phase observations; and $\Delta^s_r$ is the observation noise that is independent of frequency. Notably, the orbital altitude of LEO satellites is generally above 350 km, well above the 18 km tropospheric height, so tropospheric delay is not considered in the observation equations (Li *et al* 2019, Wang *et al* 2021).

During the operation of LEO satellites, the rapid relative motion between GNSS satellites and the onboard receiver makes the received signals susceptible to multipath effects, causing periodic drifts and significant errors. Therefore, before processing, the data should be segmented based on a specified elevation angle. Subsequently, dual-frequency pseudorange code observations (Melbourne–Wubbena combination)

and ionospheric residual observations are employed to detect cycle slips and gross errors, respectively (Jin *et al* 2012). Then, the GF combination for pseudorange and carrier phase observations at both frequencies is applied to eliminate frequency-independent terms (Liu *et al* 2020, Wang *et al* 2023),

$$\begin{aligned} P^s_{\mathrm{GF},r} &= P^s_{r,1} - P^s_{r,2} = c\mathrm{DCB}_r + c\mathrm{DCB}^s + \alpha I^s_r \\ L^s_{\mathrm{GF},r} &= L^s_{r,1} - L^s_{r,2} = B^2_{r,1,2} - \alpha I^s_r \end{aligned} \tag{2}$$

where '*GF*' refers to the geometry-free combination of observations. Pseudorange observations are affected by DCBs, while carrier phase observations include both ionospheric delay and carrier phase ambiguity frequency differences ($B^2_{r,1,2}$). The coefficient $\alpha$ represents the ionospheric delay conversion factor and is given by (Zhong *et al* 2017):

$$\alpha = 40.28 * \left(\frac{1}{f_1^2} - \frac{1}{f_2^2}\right). \tag{3}$$

Since carrier phase noise is considerably smaller than pseudorange observation noise, a carrier phase-smoothed pseudorange is employed. In continuous observation arcs without cycle slips, the phase ambiguity remains constant and is expressed as:

$$\bar{B}^s_{r,1,2} = \frac{1}{u}\sum_{k=1}^{u}\left(L^s_{\mathrm{GF},r} + \mathrm{P}^s_{\mathrm{GF},r}\right) - c\mathrm{DCB}_r - c\mathrm{DCB}^s \tag{4}$$

where $u$ represents the total number of epochs within the arc segment. By subtracting the ambiguity estimate from the carrier phase observations, the carrier phase-smoothed pseudorange is obtained,

$$P^s_{r,sm} = \frac{1}{u}\sum_{k=1}^{u}\left(L^s_{\mathrm{GF},r} + P^s_{\mathrm{GF},r}\right) - L^s_{\mathrm{GF},r} = c\mathrm{DCB}_r + c\mathrm{DCB}^s - \alpha I^s_r. \tag{5}$$

From the equation (5), it is evident that the smoothed $P^s_{r,sm}$ includes only the GNSS receiver DCB, the satellite DCB, and the slant ionospheric delay.

### 2.3. Mapping function

The thin-layer ionosphere assumption and the MF based on the topside ionospheric pierce point are used to convert STEC along the GNSS satellite observation path into VTEC (Zhong *et al* 2016). Zhong (2017) found that, in error analysis of VTEC conversion methods, the F&K model and centroid method for equivalent height are more suitable for LEO satellite receivers, while the thin-layer model and integration method are better for ground-based receivers. The F&K geometric MF (Schaer 1999) is expressed as:

$$\begin{aligned} I^s_r &= \mathrm{MF} * \mathrm{VTEC} \\ &= \frac{1 + \left(h_{\mathrm{IEH}} + R_e\right)/\left(h_{\mathrm{LEO}} + R_e\right)}{\cos z + \sqrt{\left(h_{\mathrm{IEH}} + R_e\right)^2/\left(h_{\mathrm{LEO}} + R_e\right)^2 - (\sin z)^2}} * \mathrm{VTEC}^s_r \end{aligned} \tag{6}$$

where $h_{\mathrm{IEH}}$ represents the ionospheric effective height; $R_e$ is the Earth's radius; $h_{\mathrm{LEO}}$ is the orbit height of the LEO satellite; and $z$ is the zenith angle. The ionospheric effective height for LEO satellites is determined using the centroid method based on solar activity intensity (Zhong 2017), as follows:

$$h_{\mathrm{IEH}} = \left(0.0027F_{10.7} + 1.79\right)h_{\mathrm{LEO}} - 5.52F_{10.7} + 1350. \tag{7}$$

### 2.4. DCB estimation by spherical harmonic function

The spherical harmonic function model effectively captures the temporal and spatial variations of VTEC, providing a robust and stable mathematical framework (Jin *et al* 2012). $\mathrm{VTEC}(\beta, s)$ can be expressed as (Yue *et al* 2016):

$$\mathrm{VTEC}(\beta, s) = \sum_{n=0}^{N}\sum_{m=0}^{n}\tilde{P}_{nm}(\cos\beta)\left(a_{nm}\cos ms + b_{nm}\sin ms\right) \tag{8}$$

where $\beta$ and $s$ denote the longitude and latitude of the ionospheric piercing point, respectively, $N$ is the maximum degree of the spherical harmonic expansion, $a_{nm}$ and $b_{nm}$ are the spherical harmonic coefficients to be estimated, and $\tilde{P}_{nm}(\cos\beta)$ is the normalized associated Legendre polynomial of degree $n$ and order $m$ (Jin *et al* 2012). The expression after substituting the variables is as follows:

$$P_{nm}(x) = (-1)^m\left(1 - x^2\right)^{m/2}\frac{d^m}{dx^m}P_n(x) \tag{9}$$

where $P_n(x)$ is the Legendre polynomial, which is given by: $P_n(x) = \frac{1}{2^n n!}\frac{d^n}{dx^n}(x^2 - 1)^n$. By substituting equation (8) into equation (5), the DCB estimation model is obtained as follows:

$$\begin{aligned} P^s_{r,sm} = c\mathrm{DCB}_r + c\mathrm{DCB}^s - \alpha * \mathrm{MF} * \sum_{n=0}^{N}\sum_{m=0}^{n}\tilde{P}_{nm}(\cos\beta) \\ \times \left(a_{nm}\cos ms + b_{nm}\sin ms\right). \end{aligned} \tag{10}$$

Based on equation (10), combining observations from different GNSS satellites and receivers within single epoch results in an indirect adjustment equation for that epoch, with satellite DCB, receiver DCB, and spherical harmonic coefficients as the unknown parameters:

$$Y = [B_1, B_2, B_3] \bullet X + \varepsilon. \tag{11}$$

Specifically expressed as:

$$Y=\begin{bmatrix} P^{1}_{1,sm} \\ P^{2}_{1,sm} \\ \vdots \\ P^{m}_{1,sm} \\ P^{1}_{2,sm} \\ P^{2}_{2,sm} \\ \vdots \\ P^{m}_{n,sm} \end{bmatrix}, X=\begin{bmatrix} \mathrm{d}_1 \\ \vdots \\ \mathrm{d}_n \\ D^{1} \\ \vdots \\ D^{m} \\ X_P \end{bmatrix},$$

$$\left[B_{1,(n*m)*n}\right]=\begin{bmatrix} c & 0 & \cdots & 0 \\ c & 0 & \cdots & 0 \\ \vdots & \vdots & \ddots & \vdots \\ c & 0 & \cdots & 0 \\ 0 & c & \cdots & 0 \\ 0 & c & \cdots & 0 \\ \vdots & \vdots & \ddots & \vdots \\ 0 & 0 & \cdots & c \end{bmatrix},$$

$$\left[B_{2,(n*m)*m}\right]=\begin{bmatrix} c & 0 & \cdots & 0 \\ 0 & c & \cdots & 0 \\ \vdots & \vdots & \ddots & \vdots \\ 0 & 0 & \cdots & c \\ c & 0 & \cdots & 0 \\ 0 & c & \cdots & 0 \\ \vdots & \vdots & \ddots & \vdots \\ 0 & 0 & \cdots & c \end{bmatrix},$$

$$[B_3]=\left[\alpha*\mathrm{MF}*\tilde{P}_{nm}\left(\cos\beta\right)\right] \tag{12}$$

where $n$ denotes the number of receivers DCBs (with $n = 1$ for single-system estimation and $n = 2$ for GPS + Galileo combined estimation in this study), and $m$ is the number of observed GNSS satellites (with $m$ corresponding to 32, 36, or 32 + 36). It is assumed that the DCBs of the receivers and GNSS satellites remain constant throughout the day. Observations from $t$ epochs within a day are consolidated, where $Y$ is a $(n \times m \times t) \times 1$ matrix of carrier-smoothed pseudorange obtained from GNSS observations of $n$ LEO satellite receivers over one day; $X$ is a $(n + m + (N+1)^2 \times$ *number of ionospheric coefficients)* $\times$ 1 matrix comprising the receiver DCBs of $n$ LEO satellite receivers, the DCBs of $m$ GNSS satellites and the spherical harmonic coefficients ($X_P$); the design matrix $B$ is composed of $B_1$, $B_2$ and $B_3$, where $B_1$ is $(n \times m \times t) \times n$, $B_2$ is $(n \times m \times t) \times m$, and $B_3$ is the spherical harmonic design matrix, which is expressed for the second-order spherical harmonic expansion as follows:

$$\begin{aligned} B_3 = [&\tilde{P}_{00}\left(\cos\beta^m_n\right)\tilde{P}_{10}\left(\cos\beta^m_n\right)\tilde{P}_{20}\left(\cos\beta^m_n\right) \\ &\tilde{P}_{11}\left(\cos\beta^m_n\right)\cos s^m_n\tilde{P}_{11}\left(\cos\beta^m_n\right)\sin s^m_n\tilde{P}_{21}\left(\cos\beta^m_n\right)\cos s^m_n \\ &\tilde{P}_{21}\left(\cos\beta^m_n\right)sin\, s^m_n\tilde{P}_{22}\left(\cos\beta^m_n\right)\cos 2s^m_n\tilde{P}_{22}\left(\cos\beta^m_n\right)\sin 2s^m_n] \end{aligned} \tag{13}$$

The corresponding spherical harmonic coefficients $X_P$ are:

$$X_P = \begin{bmatrix} a_{00} & a_{10} & a_{20} & a_{11} & b_{11} & a_{21} & b_{21} & a_{22} \end{bmatrix}^{\mathrm{T}}. \tag{14}$$

To distinguish between receiver and satellite DCBs and prevent rank deficiency in the least squares computation, an additional constraint is imposed: the mean DCB for each satellite system is set to 0 (Li *et al* 2019). Here, $N$ denotes the number of satellites.

$$\sum_{j=1}^{N}\mathrm{DCB}^{s,j}=0. \tag{15}$$

For a single receiver, the daily number of observations greatly exceeds the number of unknown parameters *$(n + m + (N+1)^2 \times$ number of ionospheric coefficients)*. Consequently, with these constraints, DCBs and ionospheric coefficients can be estimated using the least squares method as described above.

### 2.5. Error estimation

This study evaluates errors in both internal and external accuracy. Internal accuracy is assessed using daily differences, monthly average differences, and the overall monthly average difference between each GNSS satellite and the reference values. If CAS and DLR reference values are available, the monthly average difference and the overall monthly average difference are estimated as follows:

$$\begin{cases} X_s = \frac{\sum_{j=1}^{D} D^{s,j} - \hat{D}^{s,j}}{D} \\ \bar{X} = \frac{\sum_{s=1}^{m} |X_s|}{m} \end{cases} \tag{16}$$

where $X_s$ is the monthly average difference between the estimated DCB of satellite $s$ and the reference DCB values from the analysis center, $D$ represents the number of days, $D^{s,j}$ is the DCB estimate for satellite $s$ on day $j$, $\hat{D}^{s,j}$ is the reference DCB value for the respective satellite, $\bar{X}$ is the overall monthly average difference for all satellites within the GPS or Galileo system, and $m$ is the number of satellites in the system.

Variance is calculated as the average of the squared differences between each estimate and the mean estimate value over the period. The standard deviation (STD) $X_{\mathrm{STD}}$, which is the square root of the variance, provides a measurement stability, with a smaller $X_{\mathrm{STD}}$ indicating more stable estimates. In terms of internal precision, $X_{\mathrm{STD}}$ reflects the dispersion of the dataset and can be computed using the following formula, where $\bar{D}$ is the mean estimate value for satellite $s$ during the estimation period.

$$X_{\mathrm{STD}} = \sqrt{\frac{\sum_{j=1}^{D}\left(D^{s,j} - \bar{D}\right)^2}{D-1}}. \tag{17}$$

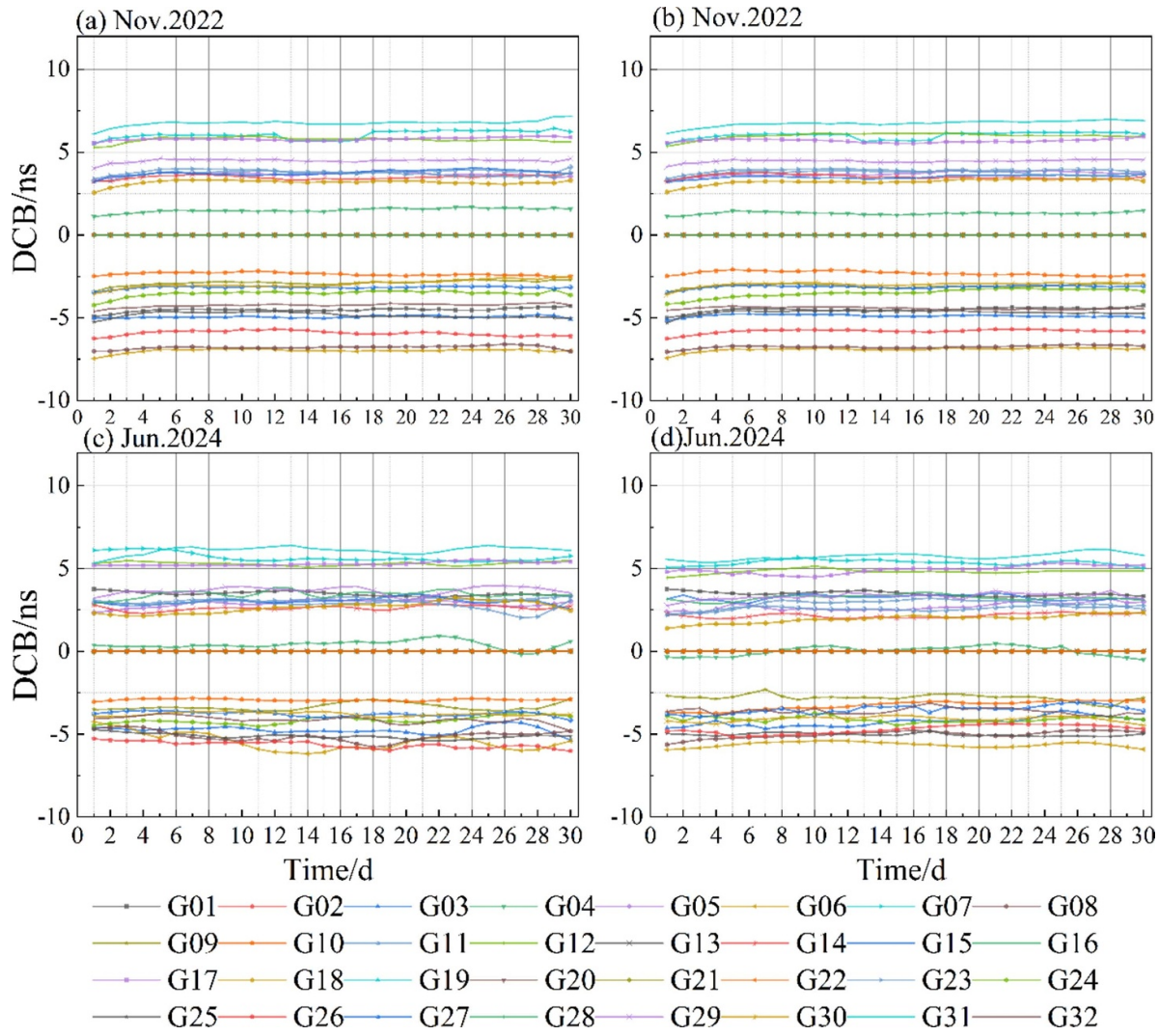


**Figure 2.** GPS satellite DCB from single system estimation (left) and combined estimation (right).

## 3. Results and analysis

GNSS receiver observation data are used from Sentinel-6A, obtained from the European Organisation for the Exploitation of Meteorological Satellites (EUMETSAT) official website (www.eumetsat.int/) in November 2022 and June 2024, to construct a fourth-order spherical harmonic function for estimating DCBs between the GPS C1C and C2L frequencies and the Galileo C1C and C5Q frequencies. The stability and reliability of spherical harmonics are validated for DCB estimation in LEO satellite GNSS receivers. The observation data have a sampling rate of 30 s and an elevation cutoff of 10°.

This study employs two types of estimations: single-system and joint GPS + Galileo estimation. Results are shown in figure 2. The evaluation includes both internal and external accuracy assessments. External accuracy is based on official data from DLR and CAS, while internal accuracy is assessed through the comparison of STDs. Note that the DCB values for GPS satellites (C1C-C2L) are not included in the products provided by CAS and DLR. These values are derived from other DCB combinations, which may introduce errors and slightly affect the precision assessment of the results.

### *3.1. Estimation of GNSS satellite DCB*

The GNSS satellite DCB is estimated from single-system and dual-system (GPS + Galileo) combined estimations for November 2022 (a), (b) and June 2024 (c), (d). Figure 2 shows that the GPS satellite DCB values range from −10 ns to 10 ns across all observation periods. All satellites exhibit small monthly variability and no apparent periodic changes, consistent with ground-based DCB estimation results. GPS + Galileo combined estimates are more stable than single-system estimates. Figure 3 presents DCB results for Galileo satellites from single-system and GPS + Galileo combined estimates. Compared to GPS satellites, Galileo satellites exhibit greater DCB variations and lower stability. Most DCBs are concentrated between −5 ns and 5 ns, with satellites E11 and E10 around 10 ns, which aligns with actual conditions. Although the GNSS satellite DCB performance in June 2024 showed greater variability due to high solar activity, with a maximum deviation of about 0.8 ns within the month, DCB results estimated from Sentinel-6A GNSS data remained consistent with ground-based observations and the product values from CAS and DLR. This consistency demonstrates the

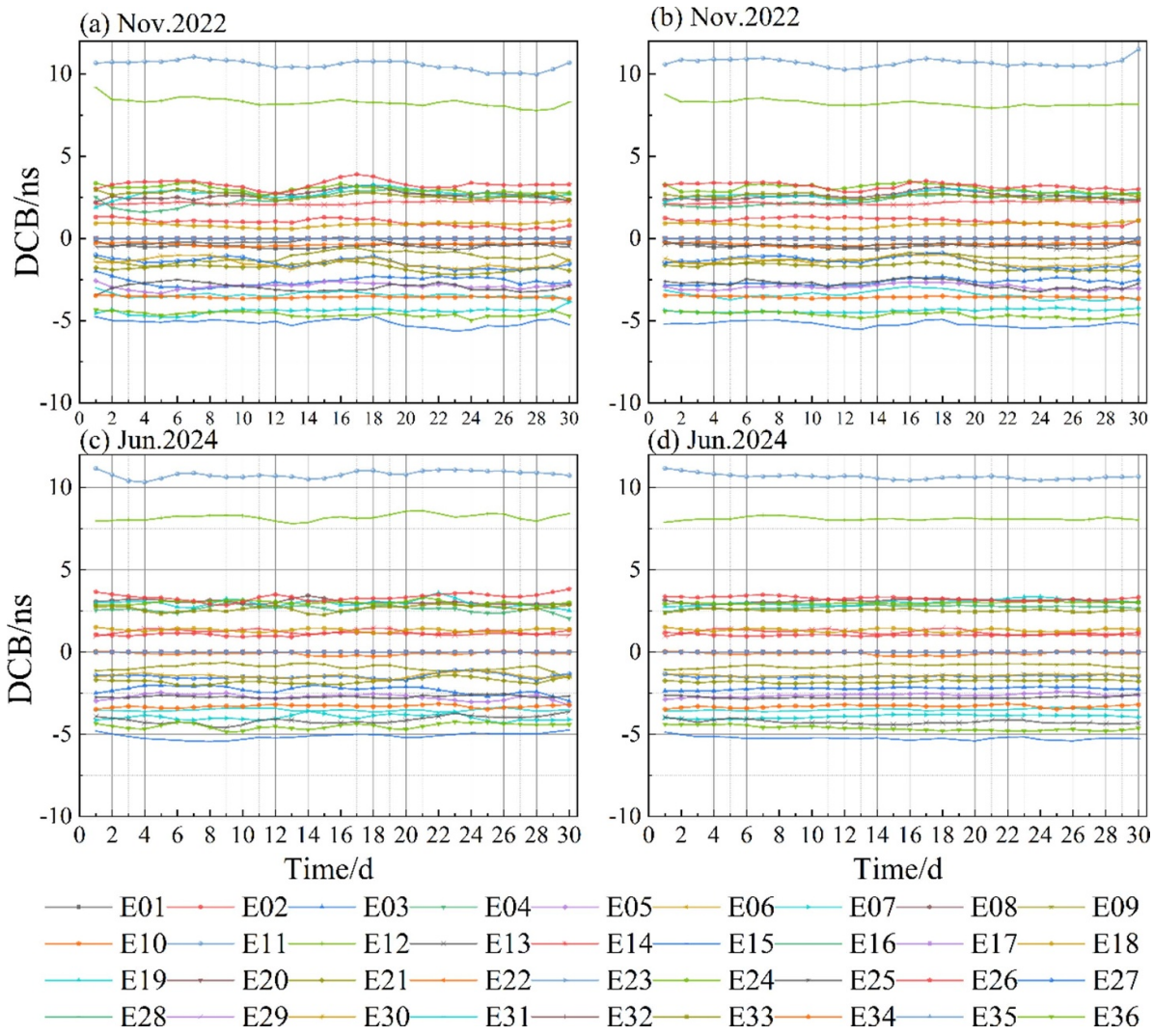


**Figure 3.** Galileo satellite DCB from single system estimation (left) and combined estimation (right).

feasibility of using Sentinel-6A GNSS data for satellite DCB estimation.

The external accuracy is evaluated by calculating the monthly average differences between the estimated DCB values for each GPS and Galileo satellite and the reference values provided by CAS and DLR (figures 4 and 5), as well as the overall monthly average differences for all satellites (table 1). CAS and DLR employ different estimation methods. CAS uses a method similar to this study, constructing an ionosphere model with high-order spherical harmonics and applying least squares to estimate the DCBs for both the receiver and the satellite. In contrast, DLR uses the global ionospheric model (GIM) to derive VTEC as the true value and then estimates the DCBs. This method for obtaining GNSS DCB products is highly dependent on GIM's ionospheric accuracy and may affect DCB estimates in localized regions (Wang *et al* 2021).

Over the 60 d observation period, the monthly average difference between the GPS satellite DCBs and the reference value is 0.8 ns (G08, G09, and G26) under stable solar activity. Under high solar activity, the difference reaches about 1 ns, slightly higher than estimates from other LEO satellite data. This discrepancy arises because CAS and DLR products exclude the DCB (C1C-C2L). This study uses related DCB combinations for true value calculations, introducing errors and resulting in a larger discrepancy between estimates and true values. For example, the average deviation for the last three satellites is 0.9 ns. Despite this, most satellite estimates demonstrate excellent performance, with a precision of $\pm$0.3 ns.

Figure 5 shows the monthly average differences between Galileo satellite DCB estimates and CAS and DLR product values for two observation periods. In the first period, the precision of Galileo satellite DCB has improved when compared to GPS satellite DCB estimates, with differences from reference values generally around $\pm$0.4 ns. Only Satellite 7 shows a notable discrepancy from DLR product values but aligns closely with CAS product values, likely due to DLR's reliance on the global ionospheric model for estimation. In the second observation period under high solar activity, the joint estimation method still performs well, and the gap between the estimated Galileo satellite DCB and the official product is below 0.3 ns.

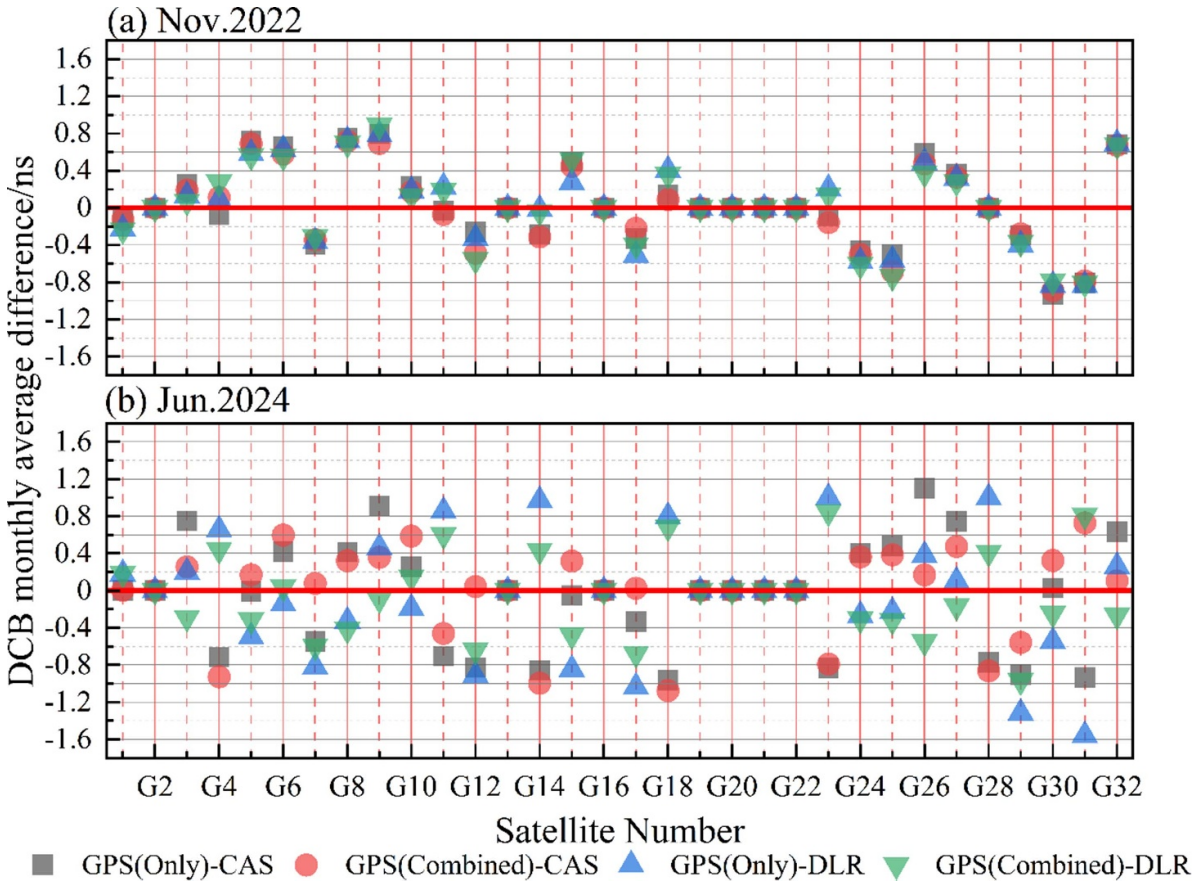


**Figure 4.** Monthly average deviation of GPS satellite DCBs from CAS and DLR products.

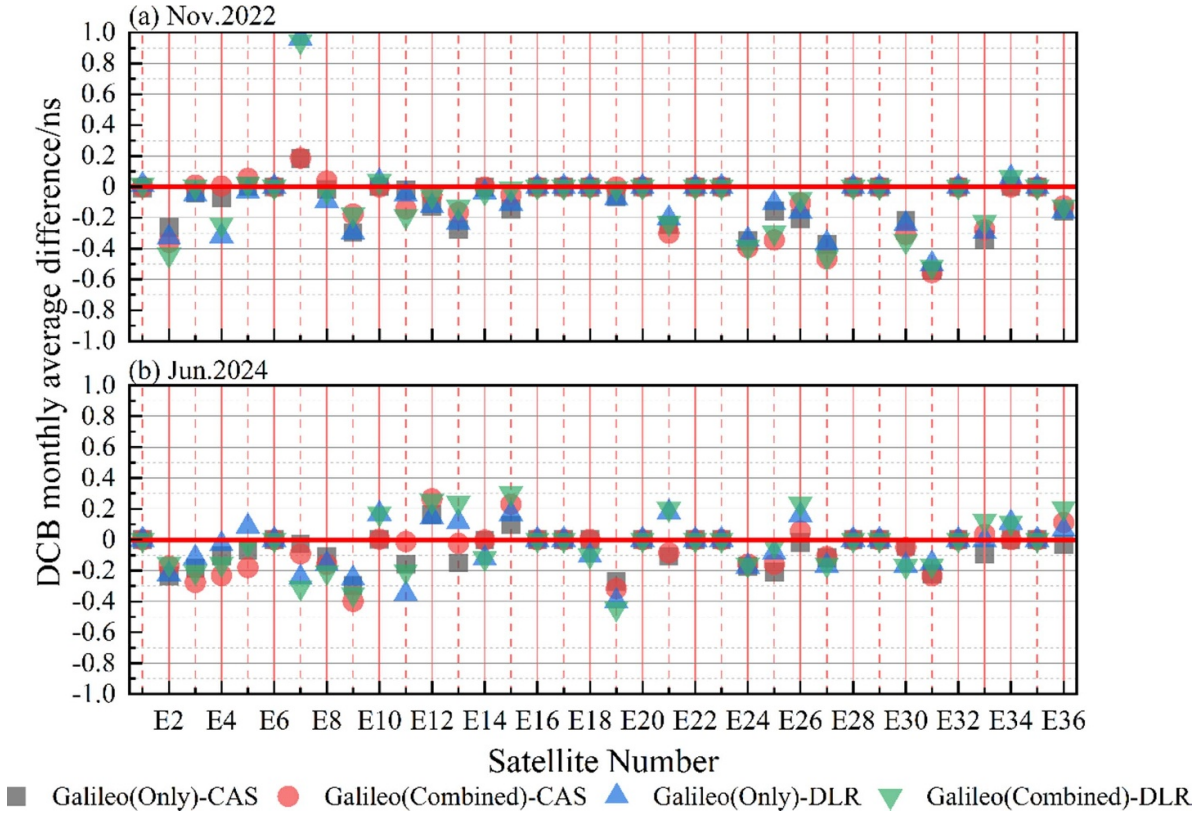


**Figure 5.** Monthly average difference of Galileo satellite DCBs from CAS and DLR products.

**Table 1.** Overall monthly average difference of satellite estimates for different observations.

| | Overall monthly average difference (ns) | | | |
|---|---|---|---|---|
| | November 2022 | | June 2024 | |
| | CAS | DLR | CAS | DLR |
| GPS (only) | 0.32 | 0.32 | 0.45 | 0.48 |
| GPS (combined) | 0.31 | 0.34 | 0.34 | 0.35 |
| Galileo (only) | 0.16 | 0.20 | 0.13 | 0.11 |
| Galileo (combined) | 0.15 | 0.19 | 0.16 | 0.19 |

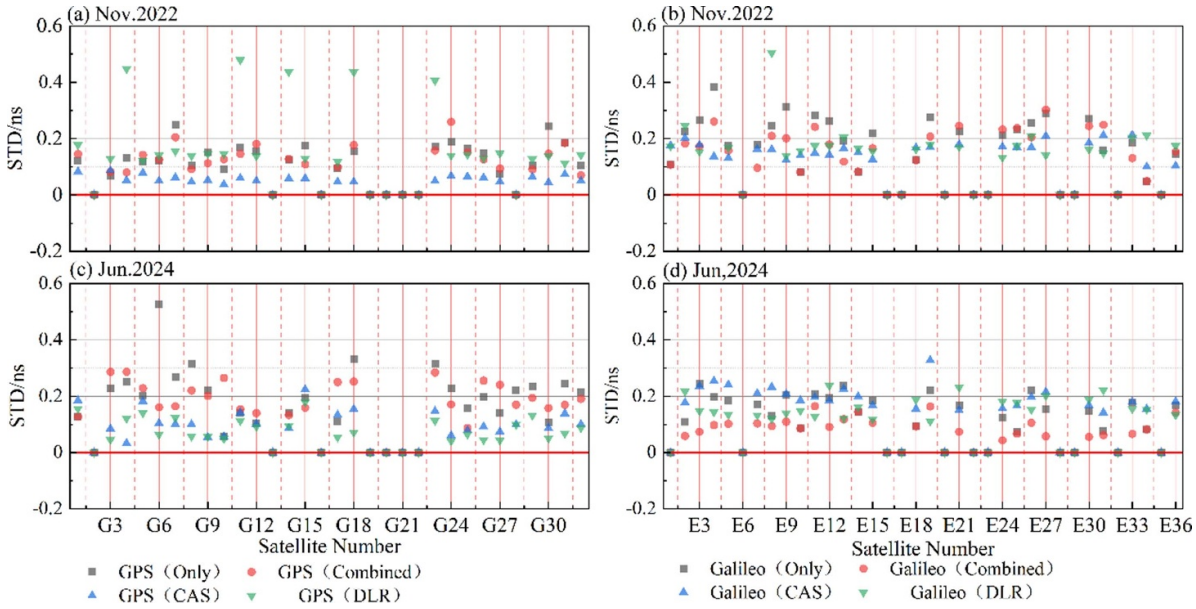


**Figure 6.** Monthly STD of satellite DCB estimates for different observations.

Table 1 shows the overall monthly average differences for satellite estimates based on different observations. Under stable solar activity (November 2022), the combined estimation results improve the accuracy for both GPS and Galileo satellites by about 10%, with differences of 0.31 ns and 0.15 ns, respectively. Adding GPS satellite observations affects the Galileo satellite DCB estimate, bringing it closer to the product value, while the joint estimate differs from CAS by only 0.15 ns. Affected by high solar activity, the accuracy of DCB estimation for the GPS satellite single system decreased in June 2024, with the overall monthly average differences of 0.45 ns and 0.48 ns from the official product values. The overall monthly average differences for the joint multi-GNSS estimation results was 0.34 ns and 0.35 ns, respectively, about 26% higher than those for single-system results. This shows that despite high solar activity, the DCB estimation for GNSS satellites using Sentinel-6A GNSS data with multi-system combined observations still performs well, especially for the Galileo satellite DCB, with a maximum difference of 0.2 ns. Compared to both product types, the results from various estimation methods are closer to CAS product values and exhibit a larger discrepancy from DLR product values, with differences up to 33%. This discrepancy arises because the spherical harmonic estimation method used in this study aligns with the CAS analysis center's method but differs from the DLR approach.

Figure 6 shows the STD of GPS and Galileo satellite DCB estimates from different observations over a 60 d period. For internal precision, during the first observation period, the STD for both single-satellite and joint estimation results ranges from 0.05 to 0.2 ns, significantly better than the STD of the DLR product value. In the second period, due to the influence of high solar activity, the monthly STD gap between satellites becomes larger, and the STD from the single-satellite estimation method increases significantly, reaching a peak of 0.5 ns. For the Galileo satellite DCB estimation, the difference between the two periods is small, and the results from the second period are even better. The results from the joint estimation algorithm are even lower than the STD of the CAS official product value, reaching below 0.1 ns. This indicates that the joint GPS and Galileo satellite observation data improve the stability of the GNSS satellite DCB estimation.

As shown in figure 6 and table 2, during the observation period of November 2022, the overall average STD from different observations remains stable at around 0.13 ns. CAS products exhibit the best performance for GPS satellite DCB, with an average STD of 0.04 ns, which significantly

**Table 2.** Overall average STD of GNSS DCBs.

| | Overall average STD of GNSS DCBs (ns) | |
|---|---|---|
| | November 2022 | June 2024 |
| GPS (only) | 0.13 | 0.23 |
| GPS (combined) | 0.12 | 0.15 |
| GPS (CAS) | 0.04 | 0.11 |
| GPS (DLR) | 0.19 | 0.07 |
| Galileo (only) | 0.21 | 0.26 |
| Galileo (combined) | 0.11 | 0.12 |
| Galileo (CAS) | 0.11 | 0.19 |
| Galileo (DLR) | 0.27 | 0.16 |

outperforms DLR's DCB products. In single-system estimation, the average STD for GPS satellite DCB is 0.13 ns. The joint estimation, leveraging more observation data, shows higher stability than single-system estimates and DLR product values, though it is slightly less accurate than CAS results. The overall average STD of joint estimation results for Galileo satellite DCB is comparable to that of CAS products. In two periods, the stability is improved by 48% and 61 %, respectively, when compared to single-system estimation reaching 0.15 ns and 0.10 ns. This indicates that including GPS data significantly enhances overall result stability. Single-system GPS estimates are also more stable than Galileo estimates, reinforcing this conclusion from a different perspective.

Overall, the GNSS satellite DCB estimation using the GPS and Galileo observation data from Sentinel-6A offers significant advantages in both internal and external accuracy when compared to single-system estimation. The GPS satellite DCB obtained from the combined estimation method is closer to the CAS product values. The average overall deviation for the two periods is 0.31 ns and 0.34 ns, respectively, with better performance under stable solar activity. The average differences between the Galileo satellite DCB obtained from the joint estimation method and the CAS product values are smaller than those of the DLR products, and the overall result exceeds the GPS accuracy. The average difference between the results of all schemes in the two periods and the CAS and DLR product values is within 0.2 ns, with the optimal value of 0.11 ns.

In terms of internal accuracy, the STD of the combined estimation results is lower than that of the single-system estimation. Incorporating GPS data into the Galileo satellite DCB joint estimate significantly reduces the STD. In both periods, the overall average STD aligns with the CAS product value and outperforms the DLR product value. Compared to single-system estimation, it is increases by 47% and 61%, respectively.

### *3.2. Estimation of GNSS receiver DCB*

The GNSS receiver on the Sentinel-6A satellite plays a crucial role in orbit determination and ionospheric modeling, but EUMETSAT has not yet published official DCB data for this receiver. Estimating the DCB for the Sentinel-6A GNSS receiver is crucial for accurate orbit determination and ionospheric modeling. This paper focuses on two key signal frequency combinations for GNSS receiver DCB estimation: the difference between the GPS L1 C/A code and the L2 P(Y) code (C1C-C2L), termed GPS receiver DCB, and the difference between the Galileo L1 C/A code and the E5 Q (or E5b) code (C1C-C5Q), termed Galileo receiver DCB.

Figure 7 shows the time series of Sentinel-6A GNSS receiver DCB in November 2022 and June 2024. Results from single-system and joint estimations are similar, showing well-fitting and consistent trends. The GPS receiver DCB remains stable at around 0.6 ns, with an initial decrease of about 0.3 ns over the first 5 days before stabilizing, and no significant periodic variations in November 2022. During the second observation period, the GPS receiver DCB shows a clear downward trend, mainly ranging from 0.5 to 2 ns. The results obtained from the combined estimation algorithm are lower, but the trend is more stable and consistent.

In contrast, the Galileo receiver DCB exhibits a fluctuating trend in mid-month, with greater overall volatility when compared to the GPS receiver DCB, around $-4$ ns in November 2022. In June 2024, both the combined and single-satellite estimates range from $-2$ to $-3$ ns, about 1 ns higher than in the first observation period, and are much less stable due to high solar activity.

Table 3 presents the monthly means and STDs of receiver DCBs for GPS (C1C-C2L) and Galileo (C1C-C5Q) using both observations. For the two observation periods, the DCB means for GPS from joint estimation differ by 0.11 ns and 0.37 ns when compared to single-system estimation, while for Galileo, the difference is 0.10 ns and 0.15 ns, indicating minimal variation.

Regarding stability, in a stable period of solar activity, the joint estimation of GPS receiver DCB performs the best, with an STD of 0.14 ns, improving by approximately 7% when compared to single-system estimates. In contrast, the Galileo receiver DCB exhibits greater stability gaps when compared to GPS, with an STD of 0.22 ns from single-system estimation and 0.15 ns for joint estimation, reflecting an improvement of about 32%. In another observation period, although the stability of the Galileo receiver DCB estimated by the single system is poor, with an STD of 0.32 ns, the stability of the results obtained from the combined estimation method using

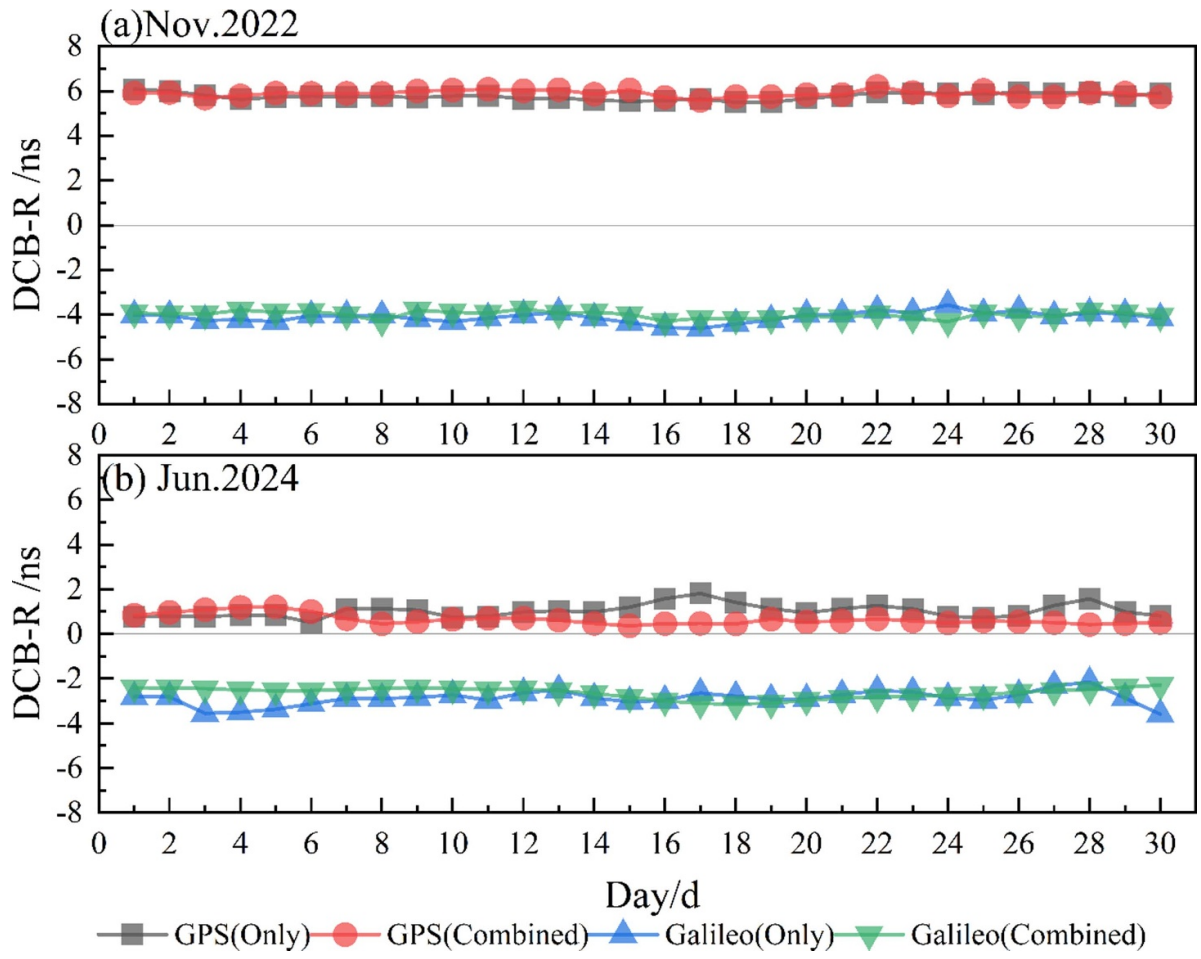


**Figure 7.** Receiver DCB results from different observations.

**Table 3.** Means and STD of receiver DCBs estimated by different observations.

| | November 2022 | | June 2024 | |
|---|---|---|---|---|
| | Average value (ns) | STD (ns) | Average value (ns) | STD (ns) |
| GPS (only) | 5.78 | 0.15 | 1.03 | 0.29 |
| GPS (combined) | 5.89 | 0.14 | 0.66 | 0.22 |
| Galileo (only) | −4.10 | 0.22 | −2.79 | 0.32 |
| Galileo (combined) | −4.00 | 0.15 | −2.64 | 0.24 |

GPS data is improved by 25%, reaching 0.25 ns. Overall, using fourth-order spherical harmonic functions for VTEC modeling offers fast computation but reduces the accuracy, resulting in receiver-end DCB STDs between 0.1 and 0.2 ns in November 2022.

### *3.3. Discussion*

This study uses GNSS data from the Sentinel-6A satellite to estimate the DCB through spherical harmonic ionosphere modeling. The DCB accuracy is assessed for LEO satellites by comparing multi-system data with single-system data from GPS and Galileo. The results show that the average absolute deviation of the GPS satellite DCB is within ±0.8 ns, while that of the Galileo satellite DCB is stable within ±0.4 ns during the two observation periods. During the stable solar activity period, the deviation between the joint estimation and the CAS value is 0.31 ns (GPS) and 0.15 ns (Galileo), while the deviation between the joint estimation and the DLR product is 0.34 ns (GPS) and 0.19 ns (Galileo). In the high solar activity period, although the gap between the results estimated by a single satellite and the product value is large, the combined estimation performance does not differ significantly from the previous period. The same holds for the estimation of Galileo satellite DCB results. This shows that, although affected by solar activity intensity, the joint estimation outperforms the single-system method, demonstrating closer consistency with CAS products. Although joint estimation demonstrates

better stability than single-system methods, it is slightly less stable than the CAS DCB products. Notably, joint estimation improves the stability of the Galileo satellite DCB and reduces the average STD by approximately 48% to 0.11 ns when compared to single-system methods. The slightly lower precision of the estimated GPS satellite DCB results is likely due to reference data from combining CAS and DLR product values, which may have caused some error accumulation. In the joint estimation scheme, the increase in data volume, the improved geometric distribution of multi-system combined satellites, and the enhancement of positioning geometry strength have significantly improved the estimation accuracy and stability of DCBs for satellites across all systems.

The estimated DCB results of the Sentinel-6A GNSS receiver show that the difference between single-system and multi-system estimation is very small. The average difference in the first period is within 0.11 ns, while in the second period, it is 0.37 ns (GPS), 0.25 ns (Galileo), and the monthly change trend is consistent. Compared to the Galileo receiver DCB results, the joint estimation results for the GPS receiver DCB show a smaller STD and greater stability. The results for November 2022 show that the smallest STD reaches 0.14 ns. The stability of the GNSS receiver DCB estimated using the joint GPS + Galileo approach is improved by 7% and 32% when compared to single-system estimates. This method provides comparable precision and stability in estimating the GNSS satellite DCBs when compared to ground-based observations and demonstrates good reliability and promising prospects for further development.

## 4. Conclusion

In this study, GPS and Galileo observation data from the Sentinel-6A satellite are used to estimate and evaluate the GNSS satellite and receiver DCB. The main conclusions are summarized as follows:

1. Multi-GNSS data significantly improves both the external and internal accuracy of GNSS satellite DCB estimation during both stable and high solar activity periods when compared to single-system data. The stability of the Galileo satellite DCB estimate even exceeds the DLR product value.
2. Including GPS data significantly improves the stability of Galileo satellite DCB estimation. During the observation period, the overall average STD is about 48% lower than that of the single-system estimation, reaching 0.11 ns.
3. The difference of the GNSS receiver DCB estimation is minimal between single-system and GPS + Galileo combined estimation, with mean differences within 0.11 ns. Using combined GPS + Galileo observations, the stability of GNSS receiver DCB estimation is 7% and 32% better than that of the single-system DCB estimation during stable solar activity.

In the future, more LEO satellites equipped with dual-frequency GNSS receivers will be launched, greatly increasing the number of GNSS observations from LEO satellites. It will further pursue detailed parameter optimization analysis for sampling rate, altitude angle, spherical harmonic function parameters, etc, and systematically evaluate accuracy differences under different parameter settings. Furthermore, non-differential, precision point positioning will be adopted for DCB estimation using additional GNSS observation data from low-earth orbit satellites, to further enhance the accuracy and stability of DCB products.

## Data availability statement

The data that support the findings of this study are openly available at the following URL/DOI: https://dataspace.copernicus.eu/.

## Acknowledgment

This work was supported by the National Natural Science Foundation of China (NSFC) Project (Grant No. 12073012). We also thanks ESA for providing GNSS observation data with https://dataspace.copernicus.eu/.

## Conflicts of interest

The authors declare no conflict of interest.

## ORCID iDs

Hui Peng https://orcid.org/0009-0002-5309-4226
Shuanggen Jin https://orcid.org/0000-0002-5108-4828
Zilong Chen https://orcid.org/0009-0004-8874-9792

## References

Jin R, Jin S and Feng G 2012 M_DCB: Matlab code for estimating GNSS satellite and receiver differential code biases *GPS Solut.* **16** 541–8
Jin S G *et al* 2024 Remote sensing and its applications using GNSS reflected signals: advances and prospects *Satell. Navig.* **5** 19
Jin S G and Li D 2018 3-D ionospheric tomography from dense GNSS observations based on an improved two-step iterative algorithm *Adv. Space Res.* **62** 809–20
Jin S G and Park J U 2007 GPS ionospheric tomography: a comparison with the IRI-2001 model over South Korea *Earth Planets Space* **59** 287–92
Jin S G, Park J, Wang J, Choi B and Park P 2006 Electron density profiles derived from ground-based GPS observations *J. Navig.* **59** 395–401
Jin S G, Wang J, Zhang H and Zhu W Y 2004 Real-time monitoring and prediction of the total ionospheric electron content by means of GPS observations *Chin. Astron. Astrophys.* **28** 331–7
Jin S G, Wang Q and Dardanelli G 2022a A review on multi-GNSS for Earth observation and emerging applications *Remote Sens.* **14** 3930
Jin S G, Wang Q and Shi Q 2022b Parameters estimation and applications from single-to five-frequency multi-GNSS precise point positioning *Acta Geod. Cartographica Sin.* **51** 1239–48
Li L and Jin S 2023 Estimation and evaluation of hourly meteorological operational (MetOp) satellites' GPS receiver

differential code biases (DCBs) with two different methods *Ann. Geophys.* **41** 465–81
Li M, Yuan Y, Zhang B and Liu M 2020 Estimation of differential code biases with Jason-2/3 onboard GPS observations *Adv. Space Res.* **67** 209–222
Li W, Li M, Shi C, Fang R, Zhao Q, Meng X, Yang G and Bai W 2017 GPS and BeiDou differential code bias estimation using Fengyun-3C satellite onboard GNSS observations *Remote Sens.* **9** 1239
Li X, Ma T, Xie W, Zhang K, Huang J and Ren X 2019 FY-3D and FY-3C onboard observations for differential code biases estimation *GPS Solut.* **23** 1–14
Li X, Zhang W, Zhang K, Zhang Q, Li X, Jiang Z, Ren X and Yuan Y 2021 GPS satellite differential code bias estimation with current eleven low earth orbit satellites *J. Geod.* **95** 76
Lin G, Wang L, He F, Song X and Guo J 2023 GPS differential code bias estimation using swarm LEO constellation onboard observations *Geomat. Inf. Sci. Wuhan Univ.* **48** 119–26
Liu M, Yuan Y, Huo X, Li M and Chai Y 2020 Simultaneous estimation of GPS P1-P2 differential code biases using low earth orbit satellites data from two different orbit heights *J. Geod.* **94** 1–18
Montenbruck O, Kunzi F and Hauschild A 2021 Performance assessment of GNSS-based real-time navigation for the Sentinel-6 spacecraft *GPS Solut.* **26** 12
Pedatella N M, Zakharenkova I, Braun J J, Cherniak I, Hunt D, Schreiner W S, Straus P R, Valant-Weiss B L, Vanhove T and Weiss J 2021 Processing and validation of FORMOSAT-7/COSMIC-2 GPS total electron content observations *Radio Sci.* **56** 1–12
Sanz J, Juan J M, Rovira-Garcia A and González-Casado G 2017 GPS differential code biases determination: methodology and analysis *GPS Solut.* **21** 1549–61
Schaer S 1999 Mapping and predicting the earth's ionosphere using the global positioning system *PhD Thesis* Geod.-Geophys. Arb. Schweiz
Shi Q, Jin S and Li L 2023 Daily plasmaspheric TEC variations from COSMIC GPS observations based on RBF neural network-kriging method *Space Weather* **21** e2022SW003347
Wang Q 2023 Study of differential code bias estimation and ionosphere modeling using multi-mode and multi-frequency GNSS observations *Acta Geod. Cartogr. Sin.* **52** 1040
Wang Q, Jin S and Hu Y 2021 Estimation and analysis of GNSS receiver differential code bias in Southeast Asia using a new method *IOP Conf. Ser.: Earth Environ. Sci.* **799** 012023
Wang Y, Liu M, Yuan Y, Wang G and Geng H 2023 Effects of topside ionosphere modeling parameters on differential code bias (DCB) estimation using LEO satellite observations *Remote Sens.* **15** 5335
Yuan L, Hoque M and Jin S 2021 A new method to estimate GPS satellite and receiver differential code biases using a network of LEO satellites *GPS Solut.* **25** 71
Yue X, Song Y, Cui X and Liu Q 2016 Single station DCB modeling algorithm based on spherical harmonics *Eng. Surv. Mapp.* **25** 16–19
Zhang X and Tang L 2014 Estimation of COSMIC LEO satellite GPS receiver differential code bias *Chin. J. Geophys.* **57** 377–83
Zhong J 2017 Investigation on the variations of the topside ionosphere using low Earth orbit satellite-based TEC *PhD Thesis*
Zhong J, Lei J, Dou X and Yue X 2016 Assessment of vertical TEC mapping functions for space-based GNSS observations *GPS Solut.* **20** 353–62
Zhong J, Lei J, Wang W, Burns A G, Yue X and Dou X 2017 Longitudinal variations of topside ionospheric and plasmaspheric TEC *J. Geophys. Res.* **122** 6737–60
Zhou P, Liu Z and Du L 2022 Estimation and analysis of GRACE-FO differential code biases *The 13th China Satellite Navigation Annual Conf. (Beijing, China)* vol 6